

Sub-millimeter propagation of antiferromagnetic magnons via magnon-photon coupling

Ryo Kainuma^{1#}, Keita Matsumoto^{1,2#}, Toshimitsu Ito³ & Takuya Satoh^{1*}

¹*Department of Physics, Tokyo Institute of Technology, Tokyo 152-8551, Japan*

²*Department of Physics, Kyushu University, Fukuoka 819-0395, Japan*

³*National Institute of Advanced Industrial Science and Technology, Tsukuba 305-8565, Japan*

*#These authors contributed equally to this study. *e-mail: satoh@phys.titech.ac.jp*

For the realization of magnon-based current-free technologies, referred to as magnonics, all-optical control of magnons is an important technique for fundamental research and application. Magnon-polariton is a coupled state of magnon and photon in a magnetic medium, which is expected to exhibit a magnon-like controllability and a photon-like high-speed propagation. Recent studies have observed magnon-polaritons as modulation of the incident terahertz wave; however, the influence of magnon-photon coupling on the magnon propagation property has not been explored. This study aimed to observe the spatiotemporal dynamics of coherent magnon-polariton through time-resolved imaging measurements. BiFeO₃ was chosen as the sample, because it is expected to exhibit strong coupling between the magnon and photon. The observed dynamics suggested that antiferromagnetic magnons can propagate over long distances up to hundreds of micrometers through strong coupling with the photons. The results shed light on the understanding of the optical control of the magnonic systems thereby paving the way for terahertz opto-magnonics.

In the past decade, research has been conducted on revolutionary information-processing devices that use magnon as an information carrier; that is, magnonics has witnessed significant progress^{1,2}. Since the study reporting spin-wave logic gate³, ferromagnetic magnons have been extensively studied. However, in recent years, the focus of research has extended from ferromagnets (FMs) to antiferromagnets (AFMs)⁴. This is mainly because of the latter's high resonance frequency up to the terahertz region. For applications, magnons must be excited coherently and propagate over a distance longer than their wavelengths to utilize superposition and nonlinearity^{2,5}. However, excitation and detection of magnons in AFMs are far more challenging than in FMs because AFMs do not exhibit net magnetization.

One of the established methods for magnon excitation is the electrical spin injection via the spin Hall effect⁶. Although applicable to AFMs⁷, it requires microfabrication and is unsuitable for coherent excitation owing to the lack of a high-frequency electric source. Ultrashort light pulse can excite and detect coherent magnons in a noncontact manner without microfabrication. Previous studies have demonstrated all-optical excitation and detection of antiferromagnetic magnons and they attributed these optical excitation mechanisms to inverse magneto-optical effects^{8,9}. However, optical excitation can only address magnons in the vicinity of the Brillouin zone center or zone edge, which cannot usually propagate owing to their group velocity being approximately zero in AFMs.

The energy transfer between magnons and photons realizes their coupled states, referred to as magnon-polaritons^{10,11}. Magnon-polaritons can be excited by light and are expected to exhibit

a nonzero group velocity owing to their anti-cross-energy dispersion. However, previous studies have mainly focused on the magnonic signature of the transmitted terahertz wave, which does not have spatial resolution. Therefore, the influence of magnon-photon coupling on magnon propagation property remains unclear.

This letter reports all-optical coherent excitation and detection of magnon-polaritons in BiFeO_3 . This material is expected to exhibit strong magnon-photon coupling because the magnons are electromagnons¹². Furthermore, BiFeO_3 enabled the excitation and detection of magnon-polaritons owing to their multiferroic nature^{13,14}. Time-resolved imaging measurements revealed that the antiferromagnetic magnon in BiFeO_3 propagates over a long distance up to hundreds of micrometers in tens of picoseconds by forming magnon-polariton. Furthermore, we estimated the coupling strength, which was comparable to strong coupling and can be utilized in both classical¹⁵ and quantum information processing¹⁶.

Figure 1a shows a schematic of multiferroic order in BiFeO_3 . At room temperature, BiFeO_3 exhibits multiferroicity of ferroelectricity ($T_C = 1100$ K) and antiferromagnetism ($T_N = 640$ K). In the antiferromagnetic phase, Néel vector \mathbf{L} exhibits a cycloidal order with a period of 62 nm^{17,18}. The wavevector \mathbf{q} of the cycloidal order typically orients in $[\bar{1}10]_{\text{pc}}$, $[0\bar{1}1]_{\text{pc}}$, $[10\bar{1}]_{\text{pc}}$ directions, perpendicular to the ferroelectric polarization, $\mathbf{P}_s \parallel [111]_{\text{pc}}$. Antiferromagnetic magnons, the eigenmodes of \mathbf{L} are classified into Φ and Ψ modes, which correspond to in- and out-of-plane oscillations, respectively, relative to the plane spanned by \mathbf{P}_s and \mathbf{q} (ref. 19). The spatial periodicity of the cycloidal order folds the magnon Brillouin zone and the deviations can be expanded using

modulated plane wave solutions $\exp[-i(\mathbf{k} + n\mathbf{q}) \cdot \mathbf{r}]$; where n denotes the n th magnon Brillouin zone. This rendered the magnons with wavevectors $\mathbf{k} + n\mathbf{q}$ as being accessible via optical measurements, such as Raman^{20,21} or infrared spectroscopy^{22,23} and pump-probe measurements¹⁴. Accordingly, the magnon eigenmodes were labelled as Φ_n and Ψ_n . The eigenmodes split by higher-order perturbations were classified using subscripts, as in $\Phi_n^{(m)}$ and $\Psi_n^{(m)}$ (ref. 24).

The BiFeO₃ single crystal was cut in (111)_{pc} plane. Figure 1b shows the ferroelectric domain structure of the BiFeO₃ sample observed using a CMOS camera under crossed-Nicols conditions. The gray regions in the red square frames did not exhibit optical birefringence, indicating \mathbf{P}_s was homogeneously perpendicular to the surface in this region. The region inside the frame was selected for performing the observations.

Pump-probe imaging measurements for BiFeO₃ were performed using femtosecond laser pulses with durations of 60 fs. A linearly polarized pump pulse of wavelength 1300 nm was focused on the sample as a line-shaped spot with a width of approximately 20 μm . The pump pulses were irradiated to the left edge of the region shown in Fig. 1b. Moreover, the probe pulse was irradiated at a wavelength of 800 nm without focusing and with time delays relative to the pump pulse. An optical configuration that is sensitive to the off-diagonal component of the refractive index modulation was adopted to facilitate selective extraction of extraordinary electromagnetic waves²⁵. For details on the detection scheme, see the Methods section.

Figure 2a and Supplementary Movie 1 shows the spatiotemporal waveform observed in the pump-probe imaging experiment. As evident, the wavepackets propagated outside the pump spot

at $x = 0 \mu\text{m}$. These wavepackets corresponded to phonon-dressed terahertz electromagnetic waves (phonon-polaritons) generated under Cherenkov-type phase matching^{25,26}. The excitation mechanism is described in the Supplementary Information. The propagation of magnon wavepackets was not clearly observed in real spacetime, the reason for which is discussed later.

A Fourier transform was applied to visualize the population of magnons and phonons in k - f space, using waveforms that were 150–945 μm from the excitation spot (the region inside the black dashed frame, as shown in Fig. 2d.). Figure 2d shows the linear dispersion of terahertz electromagnetic waves. This study selectively extracted the components with a finite group velocity when the excitation spot was excluded from the Fourier transform. Therefore, Fig. 2d contains no signals of phonons or magnons localized at the pump spot. The group velocity of the electromagnetic waves was approximately $6.1 \times 10^7 \text{ m s}^{-1}$. Thus, the corresponding refractive index was $n_{\text{THz}} = 4.9$. This value is comparable to that reported in a previous study [$n_{\text{THz}} = 5.2$ at 400 K (ref. 27)] and is greater than the refractive index for the pump pulse ($n_{\text{pump}} = 2.7$), which supports Cherenkov-type phase matching. However, anticrossings corresponding to magnon-photon coupling were not clearly identified.

We translated the Fourier transform domain in the time direction to selectively extract the components with different group velocities, as shown in Figs. 2a, 2b, and 2c. We found a specific component at $f = 0.56 \text{ THz}$ and $k = 60 \text{ rad mm}^{-1}$ increases its power significantly later than the other components, as shown in Fig. 2d, 2e and 2f in that order (See Supplementary Movie 2). Temperature-dependence measurements revealed that the frequencies at which the specific compo-

nents appeared were consistent with the frequencies of the magnon $\Psi_1^{(1)}$ mode²⁸, as shown in Fig. 2k. Thus, we conclude that this signal is located at the anticrossing point of the dispersion curves of magnon $\Psi_1^{(1)}$ mode and photons, manifesting the signal originates from magnon-polariton.

To visualize the quantitative information from the heat maps (Figs. 2d–f), first, we integrated the excitation intensities near the anticrossing in the k -direction (Figs. 2g–i). Figure 2g shows a dip at 0.56 THz, thereby supporting the idea that the magnon-polariton exhibits a relatively slower group velocity than the other nearly non-perturbed photons. Moreover, Figs. 2h and 2i show that the magnon-polaritons reached the Fourier transform region after the other components passed through. For further confirmation, we plotted the time evolution of the powers of several frequency components at $k = 60 \text{ rad mm}^{-1}$, as shown in Fig. 2j. The horizontal axis represents the start time t_a of the time domain used in the Fourier transform. The solid and dashed lines represent the time evolution of the power of each frequency component corresponding to the change in pixel brightness in Figs. 2d–f. As expected, a noticeable difference in behaviour was observed, with the magnon-polaritons of 0.56 THz component increasing later than those of the other components. The above observations confirmed that magnon-polariton exhibited group velocity in the intermediate region between the non-perturbed magnons and photons.

The coupling strength of the magnon-polariton was estimated as follows: Let $\hbar\omega_{\text{pt}}(k) = \hbar ck/n_{\text{THz}}$ and $\hbar\omega_{\text{m}}$ be the energies of the (phonon-dressed) photons and magnons in BiFeO_3 , respectively, assuming no magnon-photon coupling. By introducing coherent energy transfer with

a splitting energy of $\hbar\Omega$, the phenomenological effective Hamiltonian can be expressed as ²⁹:

$$\mathcal{H}_{\text{eff}} = \hbar \begin{pmatrix} \omega_{\text{pt}}(k) - i\kappa & \Omega/2 \\ \Omega/2 & \omega_{\text{m}}(k) - i\gamma \end{pmatrix} \quad (1)$$

where κ and γ are linewidths of photons and magnons, respectively. Diagonalizing the Hamiltonian leads to eigenfrequencies of the upper (+) and lower (−) branches of magnon-polariton

$$\omega_{\pm} = \frac{1}{2} \left(\omega_{\text{pt}} + \omega_{\text{m}} - i(\kappa + \gamma) \pm \sqrt{\Omega^2 + ((\omega_{\text{pt}} - \omega_{\text{m}}) + i(\kappa - \gamma))^2} \right). \quad (2)$$

The coupling strength was characterized by the cooperativity factor, $C = \Omega^2/(\kappa\gamma)$. For $C > 1$, the energy transfer between the different oscillators was faster than energy loss, and the hybrid system was considered to exhibit strong coupling^{29,30}. By substituting $\gamma = 3.6 \text{ GHz}$ ¹⁴ and assuming $\kappa = 12 \text{ GHz}$, which is a typical value of a similar system²⁹, we obtained the linewidth of magnon-polariton as 7.8 GHz. Considering $\Delta\omega = \omega_+ - \omega_-$ has a real part less than 16 GHz at the anticrossing point, we estimated that the upper limit of Ω as approximately 11.6 GHz and $C = 3.1$ using eq. (2). Further, the condition $\Omega^2 > (\kappa - \gamma)^2$ must be satisfied for $\Delta\omega$ to have a nonzero real part that cause the change of group velocities of magnon and photon. Under the above conditions, it follows that $8.4 \text{ GHz} < \Omega < 11.6 \text{ GHz}$ and $1.6 < C < 3.1$. This indicates the system can exist in a strong-coupling regime.

Magnon-polaritons near the anticrossing point exhibited group velocities in the range of 0– $6.1 \times 10^7 \text{ m s}^{-1}$ ($= c/n_{\text{THz}}$) depending on the wavenumbers. Assuming an average group velocity of $3.0 \times 10^7 \text{ m s}^{-1}$ for the excited magnon-polariton, as a value in the middle of this range, it can be concluded that the group velocity of the magnon-polariton is three orders of magnitude higher than that in the conventional ferromagnetic system³¹, although it is an approximate estimation.

In conclusion, this study performed time-resolved imaging measurements of BiFeO₃ and found that antiferromagnetic magnon can propagate over hundreds of micrometers via magnon-photon coupling. The analyses based on the Fourier transform revealed the wavenumber-resolved information inaccessible by conventional THz-spectroscopy. Further, the refractive index of BiFeO₃ n_{THz} were extracted and the approximate value of the splitting frequency and group velocity of magnon-polaritons were determined. Although we observed data using an unprocessed single crystal, future extensions such as coupling enhancement by a cavity optomagnonic system are possible³². Thus, our findings provide comprehensive insights into antiferromagnetic magnonics, polaritonics, and future applications.

Acknowledgements

We thank K. T. Yamada for the valuable discussions and technical support. T.S. was financially supported by the Japan Society for the Promotion of Science (JSPS) KAKENHI (grant nos. JP19H01828, JP19H05618, JP19K21854, JP21H01032 and JP22H01154), and Frontier Photonic Sciences Project of the National Institutes of Natural Sciences (grant nos. 01212002 and 01213004). R.K. was supported by JSPS KAKENHI (Grant No. JP22J20939).

Author contributions

T.S. conceived and supervised the study. R.K. and K.M. performed the experiments and analyzed the data. T.I. fabricated samples. R.K. wrote the manuscript. All the authors discussed the results and commented on the manuscript.

1. Kruglyak, V. V., Demokritov, S. O. & Grundler, D. Magnonics. *J. Phys. D: Appl. Phys.* **43**, 264001 (2010).
2. Pirro, P., Vasyuchka, V. I., Serga, A. A. & Hillebrands, B. Advances in coherent magnonics. *Nat. Rev. Mater.* **6**, 1114–1135 (2021).
3. Schneider, T. *et al.* Realization of spin-wave logic gates. *Appl. Phys. Lett.* **92**, 022505 (2008).
4. Baltz, V. *et al.* Antiferromagnetic spintronics. *Rev. Mod. Phys.* **90**, 015005 (2018).
5. Chumak, A. V. *et al.* Advances in magnetics roadmap on spin-wave computing. *IEEE Trans. Magn.* **58**, 1–72 (2022).
6. Hirsch, J. Spin Hall effect. *Phys. Rev. Lett.* **83**, 1834 (1999).
7. Lebrun, R. *et al.* Tunable long-distance spin transport in a crystalline antiferromagnetic iron oxide. *Nature* **561**, 222–225 (2018).
8. Satoh, T. *et al.* Spin oscillations in antiferromagnetic NiO triggered by circularly polarized light. *Phys. Rev. Lett.* **105**, 077402 (2010).
9. Němec, P., Fiebig, M., Kampfrath, T. & Kimel, A. V. Antiferromagnetic opto-spintronics. *Nat. Phys.* **14**, 229–241 (2018).
10. Mills, D. L. & Burstein, E. Polaritons: the electromagnetic modes of media. *Rep. Prog. Phys.* **37**, 817 (1974).
11. Grishunin, K. *et al.* Terahertz magnon-polaritons in TmFeO₃. *ACS Photonics* **5**, 1375–1380 (2018).

12. Rovillain, P. *et al.* Electric-field control of spin waves at room temperature in multiferroic BiFeO₃. *Nat. Mater.* **9**, 975–979 (2010).
13. Fiebig, M., Lottermoser, T., Meier, D. & Trassin, M. The evolution of multiferroics. *Nat. Rev. Mater.* **1**, 1–14 (2016).
14. Khan, P., Kanamaru, M., Matsumoto, K., Ito, T. & Satoh, T. Ultrafast light-driven simultaneous excitation of coherent terahertz magnons and phonons in multiferroic BiFeO₃. *Phys. Rev. B* **101**, 134413 (2020).
15. Aspelmeyer, M., Kippenberg, T. J. & Marquardt, F. Cavity optomechanics. *Rev. Mod. Phys.* **86**, 1391–1452 (2014).
16. Imamoglu, A. *et al.* Quantum information processing using quantum dot spins and cavity QED. *Phys. Rev. Lett.* **83**, 4204–4207 (1999).
17. Sosnowska, I., Neumaier, T. P. & Steichele, E. Spiral magnetic ordering in bismuth ferrite. *J. Phys. C: Solid State Phys.* **15**, 4835–4846 (1982).
18. Burns, S. R., Paull, O., Juraszek, J., Nagarajan, V. & Sando, D. The experimentalist’s guide to the cycloid, or noncollinear antiferromagnetism in epitaxial BiFeO₃. *Adv. Mater.* **32**, 2003711 (2020).
19. de Sousa, R. & Moore, J. E. Optical coupling to spin waves in the cycloidal multiferroic BiFeO₃. *Phys. Rev. B* **77**, 012406 (2008).

20. Cazayous, M. *et al.* Possible observation of cycloidal electromagnons in BiFeO₃. *Phys. Rev. Lett.* **101**, 037601 (2008).
21. Rovillain, P. *et al.* Polar phonons and spin excitations coupling in multiferroic BiFeO₃ crystals. *Phys. Rev. B* **79**, 180411 (2009).
22. Talbayev, D., Lee, S., Cheong, S.-W. & Taylor, A. J. Terahertz wave generation via optical rectification from multiferroic BiFeO₃. *Appl. Phys. Lett.* **93**, 212906 (2008).
23. Komandin, G. A. *et al.* Optical properties of BiFeO₃ ceramics in the frequency range 0.3–30.0 thz. *Phys. Solid State* **52**, 734–743 (2010).
24. Farkas, D. G. *et al.* Selection rules and dynamic magnetoelectric effect of the spin waves in multiferroic BiFeO₃. *Phys. Rev. B* **104**, 174429 (2021).
25. Matsumoto, K. & Satoh, T. Selective imaging of the terahertz electric field of the phonon-polariton in LiNbO₃. *Phys Rev. B* **102**, 094313 (2020).
26. Auston, D. H. Subpicosecond electro-optic shock waves. *Appl. Phys. Lett.* **43**, 713–715 (1983).
27. Białek, M., Ito, T., Rønnow, H. & Ansermet, J.-P. Terahertz-optical properties of a bismuth ferrite single crystal. *Phys. Rev. B* **99**, 064429 (2019).
28. Białek, M., Magrez, A., Murk, A. & Ansermet, J.-P. Spin-wave resonances in bismuth orthoferrite at high temperatures. *Phys. Rev. B* **97**, 054410 (2018).

29. Sivarajah, P. *et al.* THz-frequency magnon-phonon-polaritons in the collective strong-coupling regime. *J. Appl. Phys.* **125**, 213103 (2019).
30. Hioki, T., Hashimoto, Y. & Saitoh, E. Coherent oscillation between phonons and magnons. *Commun. Phys.* **5**, 1–8 (2022).
31. Mahmoud, A. *et al.* Introduction to spin wave computing. *J. Appl. Phys.* **128**, 161101 (2020).
32. Parvini, T. S., Bittencourt, V. A. S. V. & Kusminskiy, S. V. Antiferromagnetic cavity optomagnonics. *Phys. Rev. Res.* **2**, 022027 (2020).

Methods

The 120- μm -thick $(111)_{\text{pc}}$ -oriented BiFeO_3 single crystal was grown using the modified floating-zone method with laser diodes³³ with magnetic annealing in $[10\bar{1}]_{\text{pc}}$ -direction. A Ti:sapphire regenerative amplifier with a repetition rate of 1 kHz and a pulse duration of $\tau = 60$ fs was used to generate both the pump and probe pulses with a central wavelength of 800 nm. Further, the central wavelength of the pump pulse was converted to 1300 nm using an optical parametric amplifier. We focused on the pump pulse on the sample in a region with a width of 20 μm using a cylindrical lens. The azimuthal angle of the linearly polarized pump pulse was rotated using a half-wave plate. The probe pulse was circularly polarized using a quarter-wave plate (QWP). Moreover, the probe pulses was elliptically polarized owing to the sample's electro-optical (EO) or magneto-optical (MO) effect of the sample. The transmitted probe pulse were transformed into an approximately linearly polarized pulse using another QWP. Further, the ellipticity change of the probe pulse was determined employing a rotating-polarizer method with wire grid analyzer and CMOS camera. The analysis method is explained in the Supplementary Information. The sample was set in a cryostat for temperature-dependent measurements from 5 to 300 K.

33. Ito, T., Ushiyama, T., Yanagisawa, Y., Kumai, R. & Tomioka, Y., Growth of highly insulating bulk single crystals of multiferroic BiFeO₃ and their inherent internal strains in the domain-switching process. *Cryst. Growth Des.* **11**, 5139–5143 (2011).

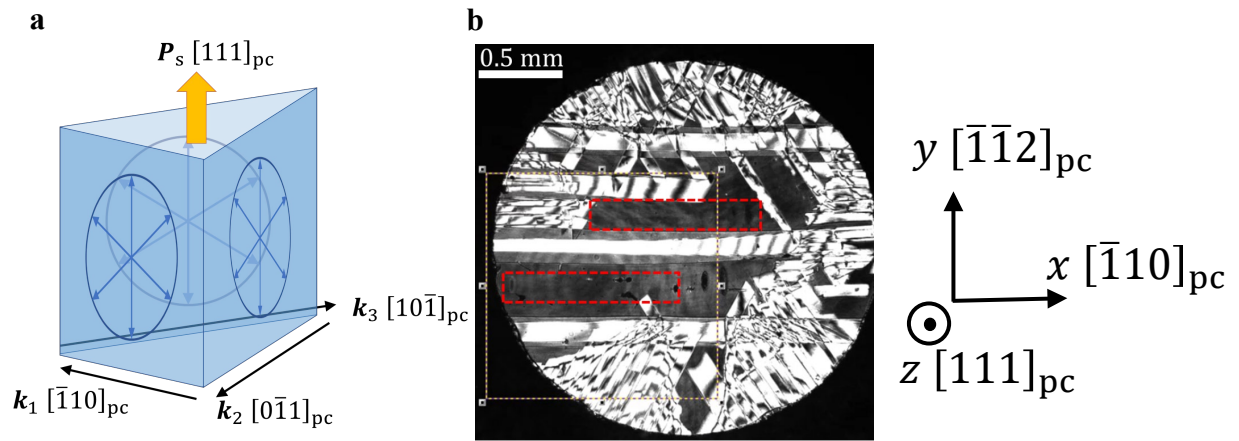


Figure 1: **Multiferroic BiFeO₃ single crystal.** **a** The schematic structure of multiferroic order of BiFeO₃. Blue bidirectional arrows shows three directional magnetic domains of the cycloidal order. **b** BiFeO₃ single crystal for our measurements. The spatiotemporal waveforms observed in the two red box were used for the analysis.

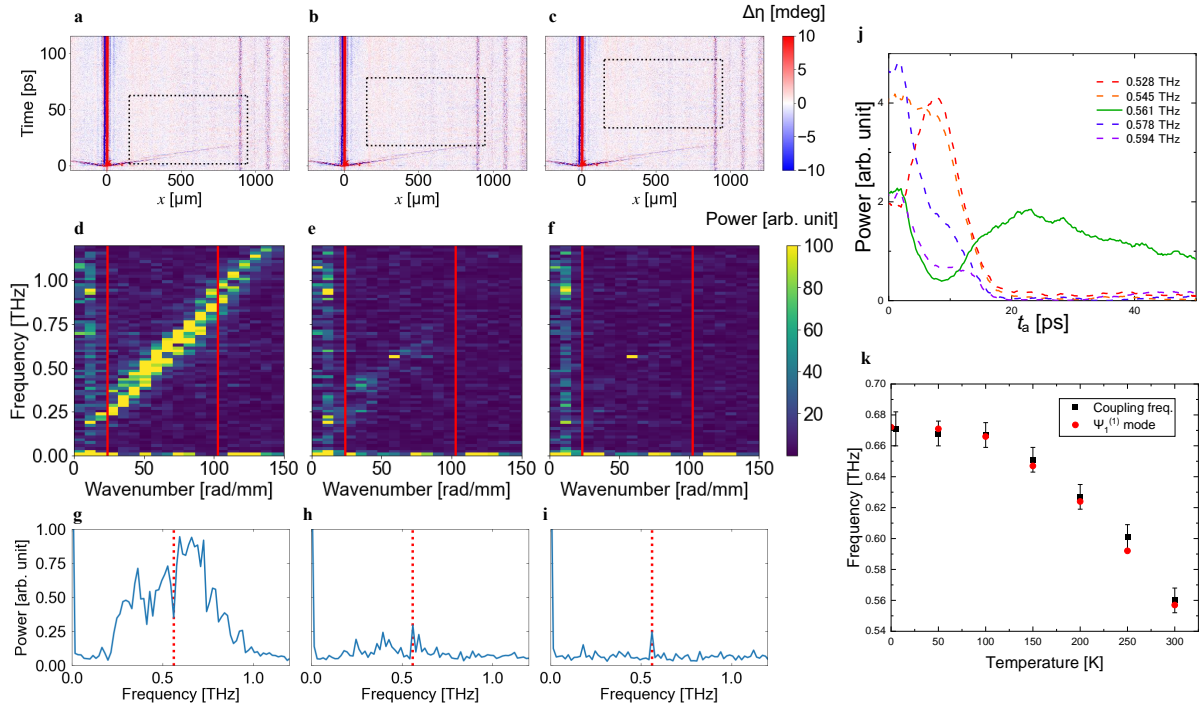


Figure 2: Coherent magnon-polariton propagation. **a** The spatiotemporal waveform observed in the pump-probe imaging measurement. The colours in the heat map painted red to blue, represent the ellipticity change of the circularly polarized probe pulse induced at each point of the sample. The black dashed frame shows the region of the Fourier transform for **d**. **b** and **c** shows the same waveform as **(a)** and different Fourier transform regions for **e** and **f**, respectively. **g–i** are distributions in **d–f** integrated in the wavenumber direction in the region between the red lines in **d–f**. The red dashed line in **g–i** represents 0.56 THz. **j** is the time evolution of the power of the components around the (anti-)crossing point. **k** is the temperature dependence of the frequency, which exhibited anomalous behaviour in **j** and the eigenfrequency of the magnon $\Psi_1^{(1)}$ mode²⁸.